A Synoptic Climatology of Episodic, Subseasonal Retractions of the Pacific Jet

SHARON C. JAFFE, JONATHAN E. MARTIN, DANIEL J. VIMONT, AND DAVID J. LORENZ

Department of Atmospheric and Oceanic Sciences, University of Wisconsin—Madison, Madison, Wisconsin

(Manuscript received 11 August 2010, in final form 19 November 2010)

ABSTRACT

Twenty-eight years of NCEP–NCAR reanalysis data are employed in a composite analysis of the structure and evolution of the large-scale circulation associated with rapid, subseasonal, westward retractions of the Northern Hemisphere Pacific jet. Nineteen Pacific jet retractions are identified in the dataset. The salient characteristics of these transitions are presented, emphasizing the structure and evolution of anomalies in the zonal wind, upper-tropospheric geopotential height, sea level pressure (SLP), and tropopause potential vorticity (PV). The composite analysis demonstrates that as the jet retracts, a transition from a dominant negative anomaly to a dominant positive anomaly across the North Pacific in both the 500-hPa geopotential height and SLP fields occurs in ~10 days. The resulting anticyclonic anomalies are sprawling and intense with SLP anomalies of nearly 20 hPa and 500-hPa geopotential height anomalies of more than 200 m. The vertical superposition of these upper- and lower-level anomalies indicates that these composite structures are equivalent barotropic. These results are also consistent with the composite 200–250-hPa Ertel PV anomaly field, in which a jet retraction event is characterized by the formation of a zonally elongated, meridionally oriented PV anomaly couplet in the central North Pacific that becomes increasingly isotropic in the jet exit region simultaneous with the retraction of the jet. Because of the large spatial scale of these events, the results are also discussed in the context of storm-track variability, the East Asian winter monsoon, and tropical diabatic heating anomalies.

1. Introduction

Since its ''discovery'' nearly 70 years ago (Reiter 1963; Bryson 1994), the jet stream has been defined as a narrow ribbon of high wind speed embedded in the upper troposphere of the midlatitude westerlies, characterized by strong lateral and vertical shears and featuring one or more velocity maxima (Reiter 1967; Glickman 2000). The Northern Hemisphere (NH) jet stream has centers of maximum intensity located over the western Atlantic and western Pacific Oceans, where hemispheric baroclinicity is maximized because of land–sea temperature contrast (Hoskins and Valdes 1990). Specifically, the NH wintertime Pacific jet extends from East Asia to the date line. The region of mean acceleration of the zonal winds over East Asia is termed the jet entrance region, and the region of mean deceleration of the zonal winds near the date line is termed the jet exit region. The boreal wintertime [November–March (NDJFM)] climatology of the Pacific jet is shown in Fig. 1. The climatology used for this study is for the period 1979–2007 and is calculated using the National Centers for Environmental Prediction (NCEP) reanalysis data (www.cdc.noaa.gov/). The Pacific jet undergoes a seasonal extension and intensification through early winter (November–January) as the Northern Hemisphere midlatitude baroclinicity increases, reaching its greatest zonal extent in February, and then retracts and weakens through March and the early spring (see Fig. 1 of Newman and Sardeshmukh 1998). The maximum intensity of the mean wintertime Pacific jet is located at approximately 35°N, 135°E, with a mean maximum wind speed of 57 m s^{-1}. Of particular interest to this study is the fact that the Pacific jet undergoes rapid, subseasonal fluctuations in its zonal extent, with the jet exit region potentially located anywhere from the western Pacific near 160°E to 120°W, off the west coast of the North American continent. Jet behavior derives from the complex interaction of a number of phenomena and associated physical processes that operate on a variety of spatial and temporal scales. Among these presumed influences on the intraseasonal variability

Corresponding author address: Jonathan E. Martin, Department of Atmospheric and Oceanic Sciences, University of Wisconsin—Madison, 1225 W. Dayton Street, Madison, WI 53706.
E-mail: jemarti1@wisc.edu

DOI: 10.1175/2010JCLI3995.1

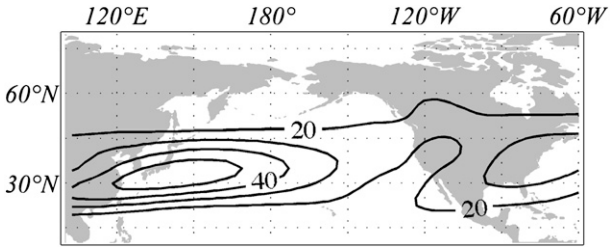

FIG. 1. Isotachs of mean zonal wind (m s^{-1}) at 300 hPa for NH winter (November–March) 1979–2007 contoured every 10 m s^{-1} beginning at 20 m s^{-1}.

of the Pacific jet are interactions between the jet and eddies comprising the storm track (Valdes and Hoskins 1989; Orlanski 1998; Chang et al. 2002); anomalies in tropical diabatic heating, such as those associated with the Madden–Julian oscillation (MJO) (Madden and Julian 1971; Hoskins and Karoly 1981; Weickmann et al. 1985; Knutson and Weickmann 1987; Madden and Julian 1994; Zhang 2005); and variability in the East Asian winter monsoon (EAWM) (Chang and Lau 1980, 1982; Lau and Li 1984; Zhang et al. 1997; Wu and Chan 1997; Wu et al. 2006).

As the primary phenomenon at the interface between transient eddies and the large-scale circulation, the jet is a particularly strong governor of regional climate. Among the notable sensible weather consequences of fluctuations in the zonal extent of the Pacific jet is a modulation of extreme precipitation events along the West Coast of the United States. Using lagged composite analysis of extreme precipitation events in eight key regions on the West Coast of the United States. Over a 49-yr period, Higgins et al. (2000) found an eastward-moving precursor region of enhanced convection migrating from the western tropical Pacific and Indian Oceans toward the central Pacific. In addition to a tropical diabatic heating connection, the composite analysis also showed that the extreme precipitation events were linked to the zonal extent of the Pacific jet, with a zonally elongated jet observed prior to the occurrence of an extreme precipitation event. Following Hoskins and Karoly (1981), they suggested that tropical heating produces a wave train moving northward and eastward into the North Pacific via its associated anomalous divergent outflow. As the tropical heating anomaly moves eastward, it acts as an eastward-moving Rossby wave source, producing a wave train whose signal is visible in the midlatitudes as an eastward extension and increased intensity of the Pacific jet. Consistent with these results, a number of studies show that a positive Pacific–North America pattern (PNA; Wallace and Gutzler 1981) and a strengthened, zonally extended jet are associated with enhanced MJO convection over the western tropical Pacific Ocean. In contrast, a negative PNA and a weakened, retracted jet occur together with enhanced MJO convection over the tropical Indian Ocean (e.g., Schubert and Park 1991; Higgins and Mo 1997; Matthews et al. 2004; Mori and Watanabe 2008; Johnson and Feldstein 2010; Moore et al. 2010).

Another example of the importance of the zonal extent of the Pacific jet is the significant influence it exerts on Hawaiian weather. Chu et al. (1993) examined two consecutive non-ENSO winters in Hawaii, looking at the average large-scale circulation in January and February of those years. The first winter (1980/81) was dry by virtue of the lack of kona storms, which account for much of the normal wintertime precipitation in Hawaii (Simpson 1952; Lyons 1982; Kodama and Barnes 1997; Otkin and Martin 2004a; Caruso and Businger 2006). The second winter (1981/82) was very wet as a result of increased kona storm activity. Chu et al. (1993) found that the dry winter was characterized by a predominantly positive PNA pattern with a zonally extended Pacific jet, and that the wet winter was characterized by a principally negative PNA pattern with a more zonally retracted Pacific jet. Subsequently, Otkin and Martin (2004b) produced a synoptic climatology of kona storms in the central subtropical Pacific using 10 yr of European Centre for Medium-Range Weather Forecasts (ECMWF) and Tropical Ocean and Global Atmosphere (TOGA) data. They reported that the Pacific jet, tied to the sign of the PNA pattern, acts as a large-scale control on kona storm activity by modulating the export of transient extratropical synoptic disturbances into the region. Inactive periods were characterized by a zonally extended Pacific jet that acted as an elongated waveguide prohibiting the equatorward propagation of midlatitude synoptic disturbances into subtropical latitudes. During active periods, the Pacific jet was more zonally retracted and acted as a ''leaky'' waveguide, allowing synoptic disturbances of extratropical origin to enter the central subtropical Pacific and spawn kona storms.

Though the Pacific jet exerts a wide and varying influence on both the sensible weather and large-scale circulation of the vast Pacific basin, the basic synoptic evolution of intraseasonal oscillations of its zonal extent are not well documented. In this paper the evolution of the large-scale environment within which rapid jet retraction events occur will be described by means of a composite analysis of such events. The paper is structured in the following way. Section 2 provides a description of the dataset and methodology used, including a detailed description of the means by which jet retraction events are identified. Results of the composite analysis are presented in section 3. A discussion of the results, which includes examination of potential mechanisms underlying jet retractions, is given along with conclusions in section 4.

2. Data and methodology

a. Data

The present study employs daily values of the horizontal wind (u, v), geopotential height (z), and sea level pressure (SLP) from 28 boreal winters (NDJFM for the period 1979/80 to 2006/07.) taken from the NCEP–National Center for Atmospheric Research (NCAR) reanalysis dataset (Kalnay et al. 1996) as well as daily values of outgoing longwave radiation (OLR) provided by the Earth System Research Laboratory (ESRL) of the National Oceanic and Atmospheric Administration (NOAA)'s Office of Oceanic and Atmospheric Research (OAR) (www.esrl.noaa.gov/psd/; Liebmann and Smith 1996). A storm-track dataset (K. Weickmann 2008, personal communication) provides pertinent records related to the life cycle of cyclones in the Northern Hemisphere (1979–2007), including the position and date of the cyclone, its central sea level pressure, and pressure tendency based on an analysis in which a local minimum of sea level pressure is used to identify cyclones in the NCEP–NCAR reanalysis dataset (Armstrong and Brodzik 1995; Serreze 1995; Serreze et al. 1997).

Daily data, subjected to a 5-day running mean to smooth out high-frequency variability, were used to identify jet retraction events. Also, to more clearly portray the large-scale structural evolution of jet retraction events, anomaly datasets were created for all variables. Anomalies were produced by subtracting the daily climatology from the smoothed daily data. The daily climatology was created in three steps. First, leap days were removed from the dataset. Second, the data were subjected to smoothing imposed by employing a 5-day running mean. Third, the daily average of the 28 yr of data was calculated.

b. Defining a jet retraction

The central element of the present analysis is sudden retractions of the Pacific jet—a phenomenon that will be referred to as a jet retraction event. In the course of this work, three methods were used to identify jet retraction events: visual inspection of the zonal wind field, analysis of the zonal wind field averaged over a region of interest, and principal component analysis.

Visual inspection identified a jet retraction event whenever the 40 m s^{-1} isotach of the 300-hPa zonal wind retreated west of 180° and remained so for a period of five or more consecutive days. The first day in such a series of days was regarded as the beginning of that retraction event and was designated as day 0 for that event. Thirty-three jet retraction events were identified in this manner (see Table 1). Though conceptually pure and analytically simple, a supplementary identification method was considered prudent.

TABLE 1. Jet retraction events as identified using the visual inspection and box-average methods (described in the text). "Year" indicates the calendar year of January–March of each season and "day no." indicates a day within that season beginning with day 1 on 1 Nov. "Wind speed departure from climatology" measures the maximum departure of the box-averaged zonal wind from its climatological value for a given retraction event, and "retraction length" is the number of days the jet remains retracted during an event. Bold rows indicate jet retraction events that are identified using both techniques.

Year	Visual inspection day no.	Visual inspection retraction length	Box-average day no. [wind speed departure from climatology (m s^{-1})]	Box-average retraction length
1980			64 (19)	10
	123	**12**	**124 (19)**	**11**
1981	112	5		
1982			73 (29)	9
			96 (27)	9
	112	**15**	**113 (25)**	**39**
1983				
1984				
1985			36 (24)	12
	96	**12**	**90 (23)**	**18**
			112 (30)	24
1986	136	11		
1987	133	5		
1988	**83**	**5**	**85 (18)**	**5**
			40 (24)	11
1989	68	6	46 (30)	32
	108	**11**	**109 (32)**	**23**
1990			73 (23)	41
	102	8	118 (25)	13
1991			11 (20)	19
			40 (22)	19
			83 (20)	7
	122	**23**	**123 (21)**	**23**
1992	**94**	**13**	**94 (24)**	**15**
1993	**40**	**35**	**40 (25)**	**40**
1994	**76**	**9**	**75 (23)**	**11**
	98	**13**	**94 (22)**	**19**
	130	**12**	**132 (21)**	**13**
1995	139	11		
1996			78 (20)	14
	105	**10**	**107 (22)**	**10**
	134	17		
1997			30 (22)	12
1998	145	6	40 (25)	40
1999	**85**	**8**	**82 (28)**	**18**
	119	**8**	**120 (22)**	**32**
	145	6		
2000			34 (18)	10
	67	**13**	**58 (30)**	**28**
2001	134	17	94 (26)	15
2002	**80**	**9**	**77 (32)**	**17**
	119	6		
2003	122	5		
2004	**135**	**6**	**133 (23)**	**11**
2005	131	15	51 (27)	22
2006	**107**	**8**	**106 (31)**	**66**
2007				9
	108	**9**	**108 (23)**	**12**
	145	6		

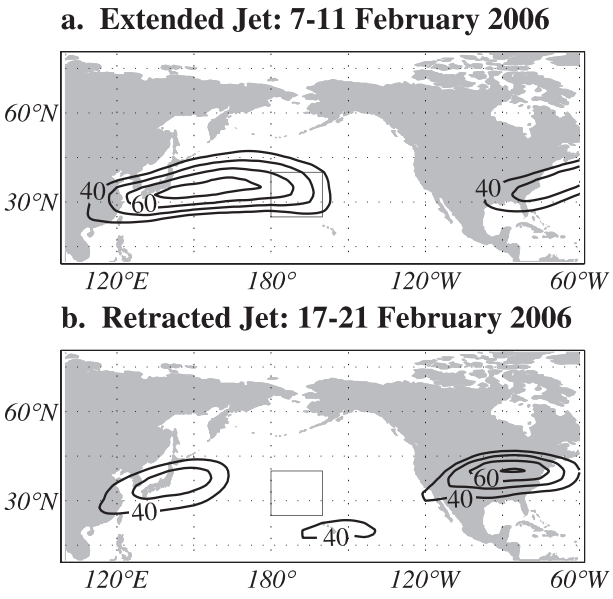

FIG. 2. Isotachs of zonal wind at 300 hPa (m s^{-1}) for actual examples of an (a) extended (7–11 Feb 2006) and (b) retracted jet (17–21 Feb 2006). Isotachs are contoured every 10 m s^{-1} starting at 40 m s^{-1}. Also shown is the box used to identify jet retraction events (25°–40°N, 180°–200°E).

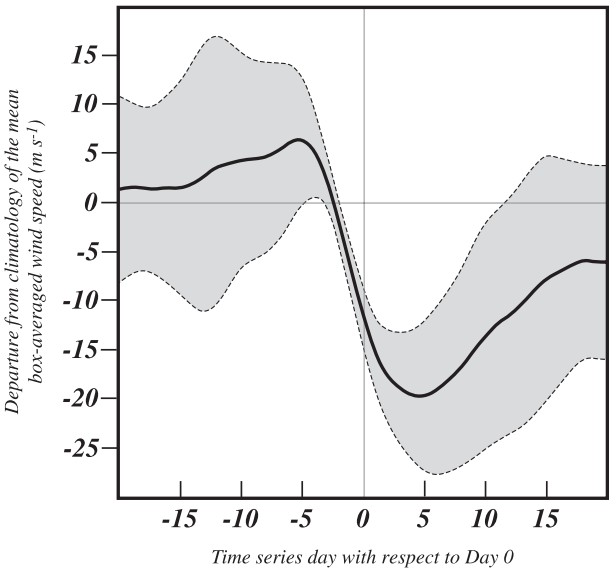

FIG. 3. Time series of the behavior of the composite zonal wind at 300 hPa. Solid line is the departure from climatology of the mean box-averaged 300-hPa zonal wind (m s^{-1}) over the 41 days comprising the analysis period for the 19 jet retraction events. Surrounding shaded area bounds the one standard deviation of the same variable for each of the 41 days comprising the analysis period for each of the 19 events.

The second method used to identify jet retractions, the "box average" method (following Reiter 1963), identified retraction events based upon the area-averaged zonal wind speed in a box defined over the central Pacific Ocean (25°–40°N, 180°–160°W). In a zonally extended jet, the jet exit region was located within the box; in a zonally retracted jet, the jet exit region was located west of the box (see Fig. 2). Using the box-average method, a jet retraction event was identified when the actual average zonal wind speed in the box was 10 m s^{-1} slower than the climatological wind speed for at least five consecutive days *and* dropped below climatology by at least 18 m s^{-1} at some point during the 5-day (or longer) period (see wind speed departure from climatology in parentheses in Table 1). The first day in such a series of days was regarded as the beginning of that retraction event and was designated as day 0 for that event. Note that the western boundary of the box was 180°, which provides a link to the visual inspection method described earlier.

Using the box-average method, 38 jet retractions were identified, 19 of which were also identified by the visual inspection method. The 15° latitudinal extent of the box used in the box-average method[1] may contribute to mistakenly classifying northward jet excursions as jet retraction events. Testing a variety of 15° latitude × 20° longitude boxes in the vicinity of the jet exit region showed that the box chosen for this analysis had the strongest relationship with the jet retraction events previously identified through visual inspection. However, given the possibility that this method could infrequently, yet nonetheless erroneously, classify northward jet excursions as jet retraction events, a conservative estimate of the number of retraction events was thought most sensible. Thus, only the 19 events that were identified in both the visual and box-average methods were used in the subsequent analysis.

Figure 3 shows a time series of the departure from climatology of the mean box-averaged zonal wind speed for all 19 retraction events bounded by the one standard deviation from the mean for each day with respect to day 0. The period encompassing 20 days before and 20 days after day 0 for each retraction event was considered. The rapidity of the jet retraction is unmistakable: the zonal wind speed is at or above its climatological value before the retraction, suddenly decreases by ~20 m s^{-1} at the retraction, and then increases toward climatological values after the retraction. Such a time series testifies to an initial jet of climatological zonal extent, which rapidly retracts and then slowly recovers back toward climatology.

[1] Reiter (1963) suggested that a box size of 15° latitude × 20° longitude is ideal for jet stream analysis, because it is large enough to eliminate the influence of shortwave disturbances but small enough to characterize the basic state of the wind field in the box separately from the large-scale circulation.

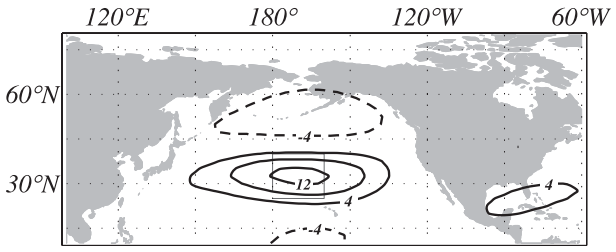

FIG. 4. Primary EOF of the 300-hPa midlatitude zonal wind field (20°–80°N) centered on the Pacific basin regressed onto the total 300-hPa zonal wind field (0°–80°N). Contours represent perturbation isotachs in units of m s^{-1}. Also shown is the box used to identify jet retraction events (25°–40°N, 180°–160°W).

The significance of jet retraction events is further supported by empirical orthogonal function/principal component (EOF/PC) analysis, applied to the 300-hPa zonal wind field. In the present study, EOF/PC analysis was applied to the 5-day running-mean 300-hPa zonal wind field over the northern Pacific Ocean (20°–80°N, 100°E–60°W) for winter (NDJFM) 1980–2007 after removing the seasonal cycle. The first PC explains 15.9% of the temporal variance in the upper-level zonal wind and is well separated from the higher-order PCs (<11% variance explained), as determined by North's rule of thumb (North et al. 1982) (also note that removing strong ENSO years had no statistically significant effect on the structure of the primary mode of variability).

The spatial structure of the primary mode of variability, shown in Fig. 4, is constructed by regressing the 300-hPa zonal wind field (0°–80°N) onto the first PC of the zonal wind (20°–80°N). The analysis shows a meridionally oriented triplet of significantly variant structures, with the center structure located at the same location as the box used in the box-average method (approximately at the mean jet exit region, shown in black outline). The structure in Fig. 4 indicates that the primary mode of variability of the zonal wind at 300 hPa is a strengthening–weakening of the zonal winds in the jet exit region. The correlation between the leading PC of 300-hPa zonal wind and the time series of the box-average zonal wind speed is $r = 0.85$, confirming that the box-average zonal wind speed is indicative of a dominant mode of variability of the upper-level zonal wind.

c. Further description of jet retraction events

To further characterize a jet retraction event, it is instructive to know whether, and to what extent, such events are indicative of a large-scale collapse of the jet; that is, are jet retraction events localized near the jet exit region, or are they coherent across the entire zonal extent of the jet? Fig. 5 depicts scatterplots of the original box-averaged zonal wind (25°–40°N) against box-averaged zonal wind anomalies in the jet entrance region (box 1, 130°–150°E, Fig. 5a), the core of the jet (box 2, 150°–170°E, Fig. 5b), and a box near the jet exit region (box 3, 170°E–170°W, Fig. 5c). Correlations between the original box-averaged wind index and wind anomalies in the box nearest to the jet exit region are large ($r = 0.88$ in box 3), decrease to $r = 0.54$ at the jet core (box 2), and decrease further to $r = 0.11$ near the jet entrance region (box 1). Therefore, it is apparent that during jet retraction events, the predominant weakening of the zonal wind speed is concentrated near the jet exit region and does not reflect a uniform weakening of the entire jet structure.

The foregoing analyses clearly establish jet retraction events as robust, relatively easy to identify features of the upper-tropospheric boreal wintertime circulation. In the following section, the composite evolution of other basic-state variables will be presented in an effort to more fully describe the large-scale characteristics of these retraction events and their possible impacts and feedbacks on the large-scale circulation and synoptic wave activity.

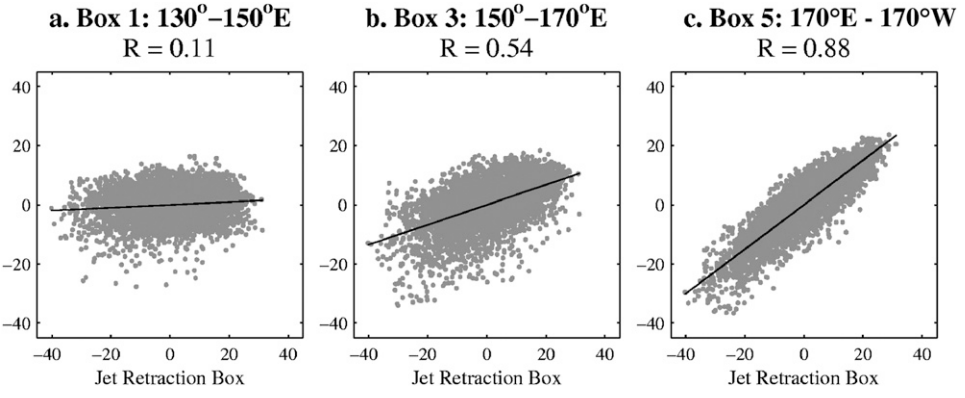

FIG. 5. Linear regression of the box-averaged zonal wind speed in boxes (a) 1, (b) 2, and (c) 3 onto the box-averaged zonal wind speed in 25°–40°N, 180°–160°W.

3. Results of the composite analysis

In this section, results from the composite analysis of the 19 jet retraction events are presented to discern the characteristic large-scale structure and evolution associated with these events. The composite analysis was performed such that the 19 jet retractions were averaged together with respect to day 0 (defined previously), forming the composite-mean jet retraction event. To capture the evolution of these events, the period encompassing 10 days before and 10 days after day 0 for each retraction event (to be referred to as day −10 and day +10, respectively) was considered. Although all 21 days of composite structure prove significant and illustrative in a full description of jet retraction events, 5 characteristic days (days −10, −5, 0, +5, +10) were chosen for display in the figures accompanying this section. The significance of the structures identified in the composites was assessed using a two-tailed Student's *t* test, and only structures that are statistically significant at the 95% confidence level will be discussed.

a. 300-hPa zonal wind

The evolution of the 300-hPa zonal wind relative to the jet retraction events is shown in Fig. 6. The extension and intensification, followed by the retraction and weakening that characterize the seasonal evolution of the Pacific jet, are evident in the composite of the subseasonal jet retraction events (Figs. 6a–e), though the time scale in the latter is greatly compressed. The jet is extended in its normal wintertime position (compared to the winter climatology in Fig. 1) at day −10 (Fig. 6a). By day −5 the 40 m s^{-1} isotach still extends beyond the date line (Fig. 6b), without much change. The jet suddenly weakens and retracts through day +5 (Figs. 6c,d). After day +5 the jet gradually begins to intensify and reextend, but the 40 m s^{-1} isotach still does not extend beyond the date line even at day +10 (Fig. 6e). It is notable that both retraction and weakening characterize these events, though variations in the jet entrance region are much smaller than those in the jet core or exit region (Fig. 5). Comparison of Fig. 6 to Fig. 1 also shows that the retraction events are not simply a relaxation to climatology; note especially that the position of the 40 m s^{-1} isotach in Fig. 1 lies east of the date line, while it lies around 165°E for the retracted jet in Figs. 6c–e.

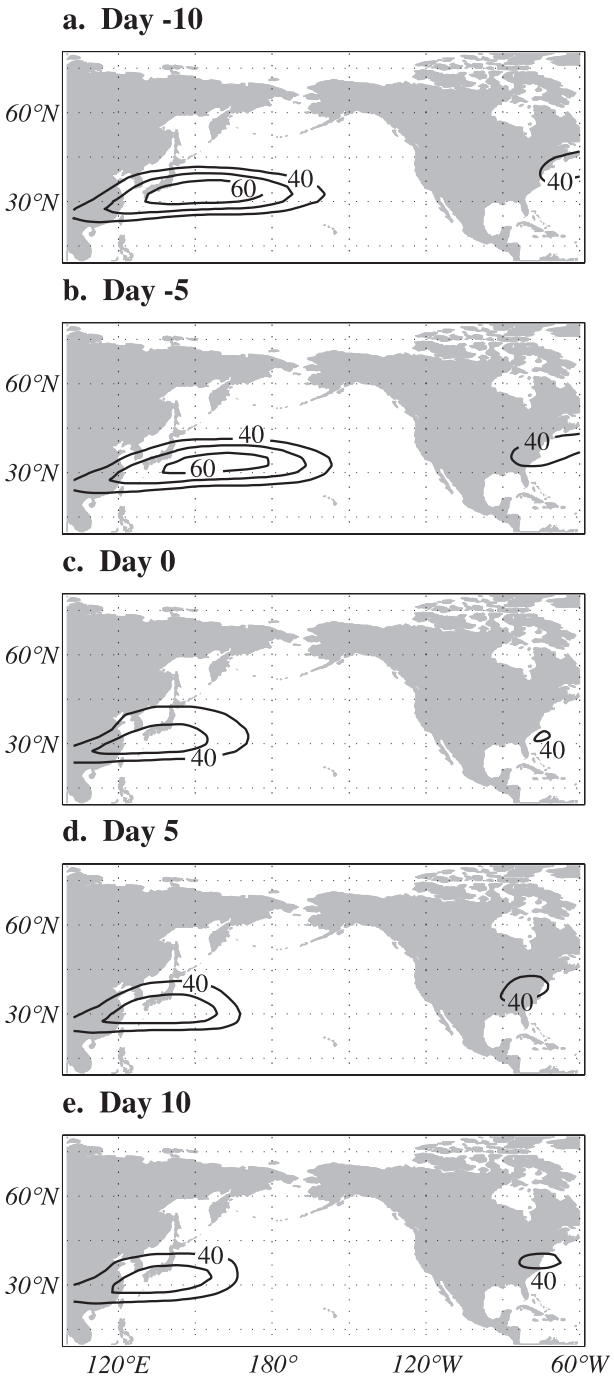

FIG. 6. Isotachs of the composite 300-hPa zonal wind (m s^{-1}) associated with a jet retraction event at days (a) −10, (b) −5, (c) 0, (d) +5, and (e) +10. Solid lines are isotachs contoured every 10 m s^{-1} starting at 40 m s^{-1}.

b. 500-hPa geopotential height

Figure 7 shows the composite structure of the associated 500-hPa geopotential height anomalies. The height field is initially characterized by an expansive negative height anomaly of −75 m that stretches over the entire midlatitude North Pacific basin at day −10 (Fig. 7a). The negative height anomaly is replaced by a growing positive height anomaly (Fig. 7c), part of which appears to originate in western North America. This feature grows rapidly between day 0 and day +5 into a 225-m positive height anomaly south of the Aleutian Islands (Fig. 7d),

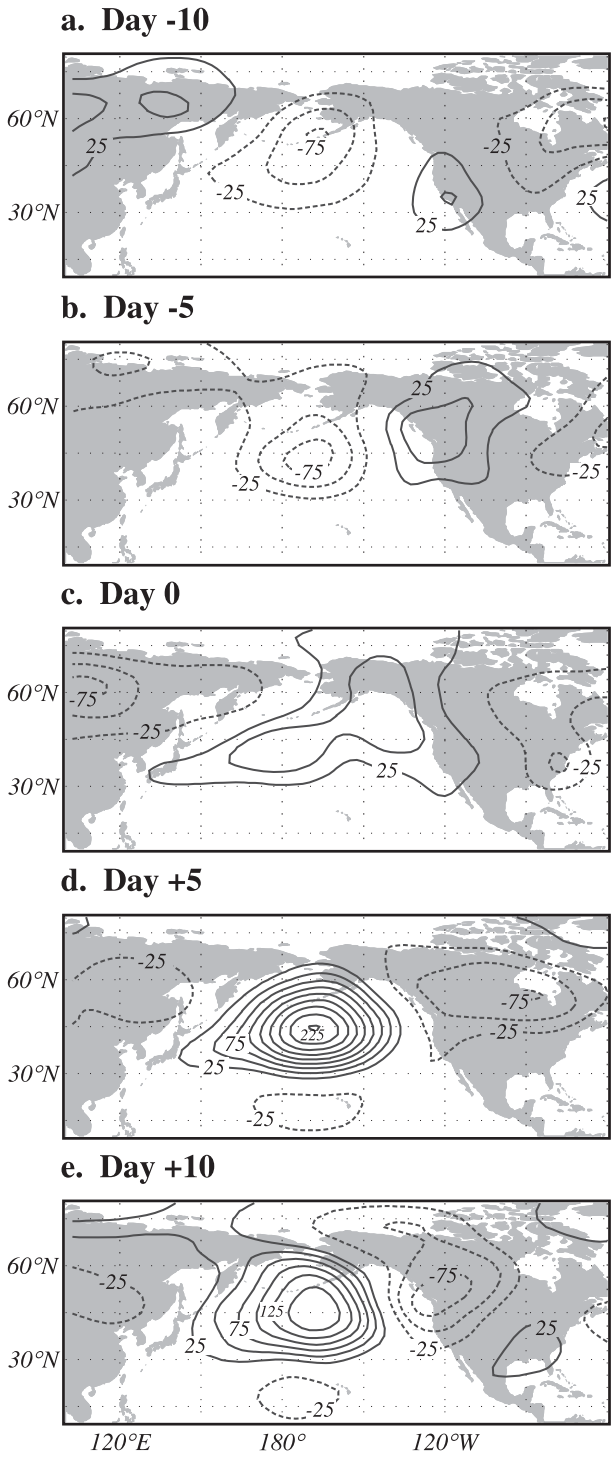

FIG. 7. As in Fig. 6, but for composite 500-hPa geopotential height anomalies (m). Solid (dashed) lines indicate positive (negative) height anomalies, contoured every 25 m with the 0 line removed.

directly poleward of a weak negative anomaly centered at 160°W. This meridional dipole of anomalous heights is associated with anomalous 500-hPa easterly geostrophic winds at 30°N in the mid-Pacific—the location of the jet axis less than two weeks earlier (see Figs. 6a,b). The pattern of geopotential height anomalies on days +5 and +10 bears a strong resemblance to the configuration of an anomalously negative PNA teleconnection pattern (Wallace and Gutzler 1981), with positive geopotential height anomalies located over the North Pacific Ocean and the U.S. Gulf Coast region and negative geopotential height anomalies located over Alberta and Hawaii. Indeed, the large correlation ($r = 0.72$ at 0 lag and $r = 0.74$ at 1-day lag) between the box-average zonal wind speed and the daily PNA index confirms that jet retraction events are strongly related to variations in the PNA pattern.

c. *Sea level pressure*

A transformation broadly similar to that observed at 500 hPa occurs in the SLP composite as well (Figs. 8a–e). At day −10 an expansive, negative SLP anomaly of −6 hPa is the dominant feature in the North Pacific (Fig. 8a). This SLP anomaly gradually weakens and shrinks in areal extent by day −5 (Fig. 8b) and is eventually replaced by a modest positive SLP anomaly centered at 35°N, 160°W by day 0 (Fig. 8c). A dramatic intensification and scale expansion of this positive SLP anomaly occurs in the following days such that by day +5, a sprawling positive SLP anomaly of nearly 20 hPa dominates the central North Pacific basin (Fig. 8d). This positive SLP anomaly remains at day +10, although it is slightly weakened, with a magnitude of approximately 12 hPa (Fig. 8e). Comparing the structure and distribution of the 500-hPa geopotential height and sea level pressure anomalies suggests that these features exhibit an equivalent barotropic structure over the ocean, consistent with the PNA teleconnection pattern (Hsu and Wallace 1985). Thus, jet retraction events are associated with a seesaw in anomalies (both SLP and geopotential height at 500 hPa) that involve a complete sign reversal of the basinwide extratropical circulation features within a 2-week period as well as an anomalously negative PNA index.

d. *Ertel PV*

An alternative view of jet retraction events is afforded by an examination of the associated composites of the 200–250-hPa Ertel potential vorticity field shown in Fig. 9. The first feature of interest in this composite is a negative PV anomaly that appears over the southern Rocky Mountains at day −10 (Fig. 9a) and moves to the northwest, weakening slightly by day −5 (Fig. 9b).

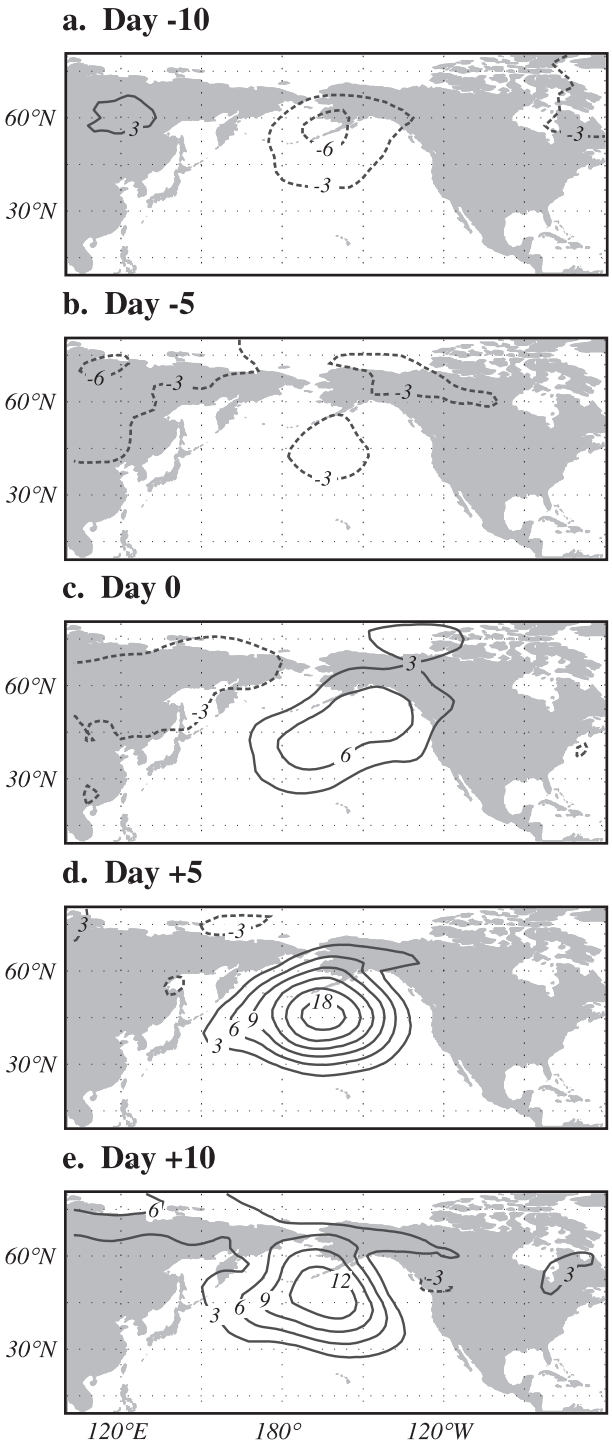

FIG. 8. As in Fig. 6, but for composite SLP anomalies (hPa). Solid (dashed) lines indicate positive (negative) SLP anomalies contoured every 3 hPa with the 0 line removed.

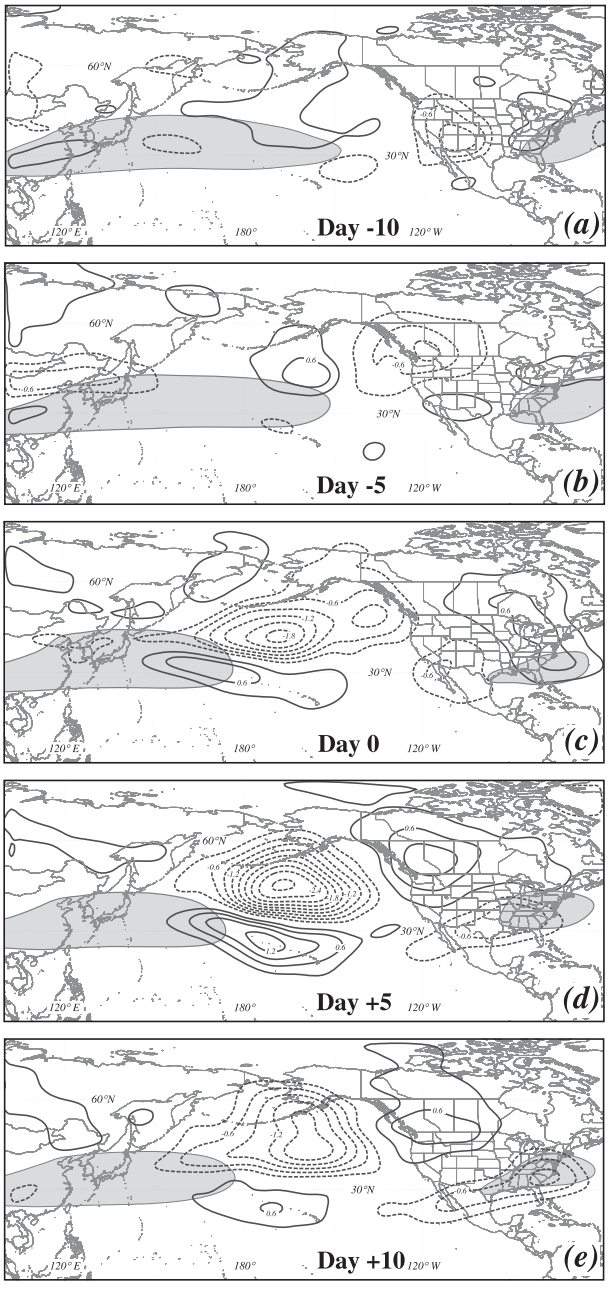

FIG. 9. As in Fig. 6, but for the composite perturbation 200–250-hPa Ertel PV. Solid (dashed) lines indicated positive (negative) perturbation PV, contoured every 0.3 PVU (1 PVU = 10^{-6} m^2 K kg^{-1} s^{-1}) with the 0 line removed. Gray shading represents the 40 m s^{-1} isotach of the composite 250-hPa zonal wind.

Meanwhile a negative PV anomaly originating over Mongolia (Fig. 9a) moves eastward along the jet (Fig. 9b) and intensifies as it is stretched along the jet axis. Examination of daily PV anomaly data (not shown) suggests that between day −5 and day 0 these two negative PV anomalies merge, with the Rocky Mountain anomaly retrogressing westward and the Mongolian anomaly moving into the jet exit region (Figs. 9b,c). As these negative PV anomalies merge they also amplify, forming a zonally elongated negative PV anomaly in the northern jet exit region by day 0 (Fig. 9c).

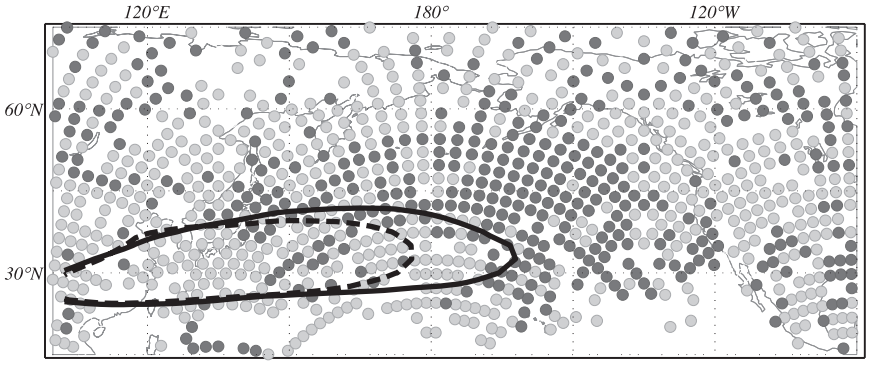

FIG. 10. Difference in storm-track density associated with the composite jet retraction event (after − before) and the mean 40 m s^{-1} contour of the zonal wind before and after the event. Dark (light) gray signifies that more storms occur before (after) a jet retraction event at a particular grid point. The solid (dashed) black lines show the 40 m s^{-1} isotach of the composite 300-hPa zonal wind before (after) a jet retraction as in Fig. 6.

A similar progression involving two positive PV anomalies located to the south of the jet core occurs. A weak positive PV anomaly originates over China at day −10 (Fig. 9a) and moves eastward through the jet axis (not shown), while a small positive PV anomaly originating west of the California coast at day −10 (Fig. 9a) moves westward toward Hawaii (Fig. 9b). Examination of daily PV anomaly data (not shown) raises the possibility that these two positive anomalies merge between day −5 and day 0 (Figs. 9b,c) while centered immediately to the west of Hawaii, leading to a zonally elongated positive PV anomaly located in the southern jet exit region, directly to the south of the developing negative PV anomaly by day 0 (Fig. 9c). The meridional juxtaposition of these PV anomalies forms a large-scale, north–south PV anomaly couplet in the central Pacific basin at day +5 (Fig. 9d). Both the negative and positive PV anomalies change shape between day 0 and day +5, becoming less zonally elongated and more isotropic (Figs. 9c,d). This is likely a result of the strongly deformative flow in the diffluent jet exit region, which acts to stretch the PV anomalies meridionally, making them more isotropic and more intense via the principle of superposition (Hoskins et al. 1985). The development of this couplet implies anomalous easterly flow in the central Pacific consistent with a retraction of the Pacific jet. Given that these initially linear PV anomalies (Fig. 9c) are rapidly deformed into more isotropic ones by day +5 (Fig. 9d), it is likely that interactions between the PV anomalies and the circulations associated with the jet exit region are fundamental to initiating jet retraction events.

e. Storm tracks

Using the previously described storm-track dataset (K. Weickmann 2008, personal communication), cyclones were identified as local sea level pressure minima of 1010 hPa or less. A storm-track density was then calculated, where the number of storms crossing each grid box was computed for periods encompassing 20 days before and after a jet retraction event. Long-lived storms that were present both before and after the jet retracted were not counted, to avoid double-counting errors. The difference in storm-track density between those two periods is shown in Fig. 10, where dark (light) gray circles indicate that more storms passed through a given point before (after) the jet was retracted. After the jet is retracted, there is a notable reduction in storm-track density downstream and poleward of the location of the original jet, to the south of the Aleutian Islands. Another region of distinct change in the storm-track density is located in the central subtropical Pacific (near 30°N, 180°E). In this location there is an increase in storm-track density after the jet retraction occurs (Fig. 10), corroborating the relationship between the zonal extent of the jet and subtropical cyclone activity presented in Otkin and Martin (2004b). In general, Fig. 10 illustrates a shift in storm activity from the eastern Pacific (prior to the jet retraction) to the central Pacific (after the retraction).

f. East Asian winter monsoon

Two indices used to identify the EAWM were produced by Jhun and Lee (2004, hereafter JL04) and Zhu (2008, hereafter Z08):

$$\mathrm{EAWMI}_{\mathrm{JL04}} = \overline{U}_{300}(27.5°\mathrm{N}-37.5°\mathrm{N}, 110°\mathrm{E}-170°\mathrm{E}) - \overline{U}_{300}(50°\mathrm{N}-60°\mathrm{N}, 80°\mathrm{E}-140°\mathrm{E}) \quad \text{and} \tag{1}$$

$$\mathrm{EAWMI}_{\mathrm{Z08}} = \overline{U}_{500}(25°\mathrm{N}-35°\mathrm{N}, 80°\mathrm{E}-120°\mathrm{E}) - \overline{U}_{500}(50°\mathrm{N}-60°\mathrm{N}, 80°\mathrm{E}-120°\mathrm{E}). \tag{2}$$

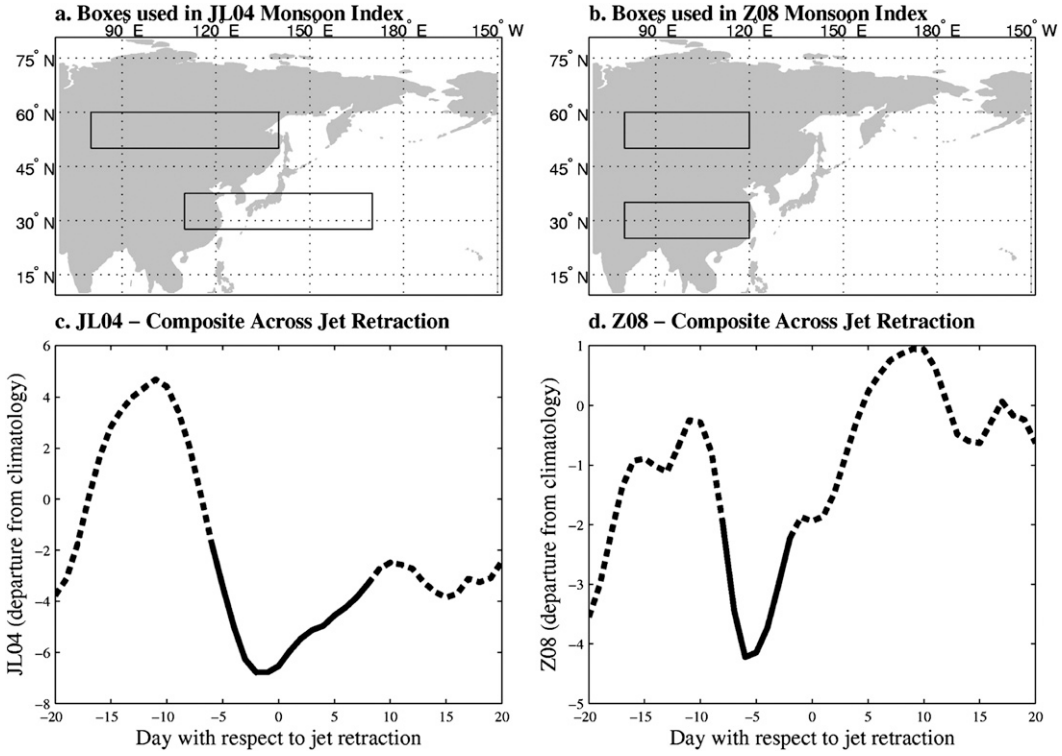

FIG. 11. Latitude–longitude boxes used for creating the JL04 and Z08 indices are shown in (a) and (b), respectively. (c) Time series of JL04 EAWM index over the composite jet retraction event (significant where solid). (d) As in Fig. 11c, but for the Z08 EAWM index.

Overbars indicate an average over the indicated box (boxes are shown in Figs. 11a,b), and U is the zonal wind speed observed at the subscripted level. The JL04 monsoon index is strongly related to the 300-hPa wind anomalies that are part of the monsoon circulation, while the Z08 monsoon index is intended to most accurately describe rapid surface temperature changes associated with cold surges in China during winter. Both indices are extremely effective at indicating when cold surge–break periods occur in the EAWM (JL04; Z08), with positive (negative) index values indicating a cold surge (break) period. These indices provide a straightforward way to test whether jet retraction events are associated with the EAWM.

Figure 11 shows composite analyses of the two standardized EAWM indices over the 19 jet retraction events. The composite of JL04 (Fig. 11c) is similar to the composite of the box-averaged zonal wind (Fig. 3), with positive index values prior to a jet retraction quickly decreasing to a minimum of −7 at day −3 and staying negative through the remainder of the period. Using the two-tailed Student's t test to gauge the significance of the composite average, the analysis shows that the JL04 composite is significant between day −5 and day +10 (Fig. 11c), implying that a large portion of the rapid decrease in JL04 index is indeed significant. According to the JL04 composite, jet retraction events are strongly related to break periods in the EAWM. A different representation of the EAWM is portrayed using Z08 (Fig. 11d). This index portrays a noisy, predominantly negative (monsoon ''break'') signal that is only briefly significant around day −5. Significant excursions of the Z08 index tend to peak slightly earlier than, and do not persist as long as, the JL04 index. Further analysis (not shown) shows that the composites for both indices are dominated by variations in their respective southern boxes. Linear regression and lag correlation analyses (not shown) were also performed and indicated weak correlations between the EAWM indices (especially Z08) and jet retractions. A modestly significant connection between the EAWM and jet retractions was found when the monsoon break leads the jet retraction by approximately one week. The lagged correlation analyses, combined with the different timings of significant relationships with the EAWM indices, suggests that jet retraction events may involve signals that propagate downstream from the EAWM area to the jet exit region, consistent with the results of a recent study by Mori and Watanabe (2008).

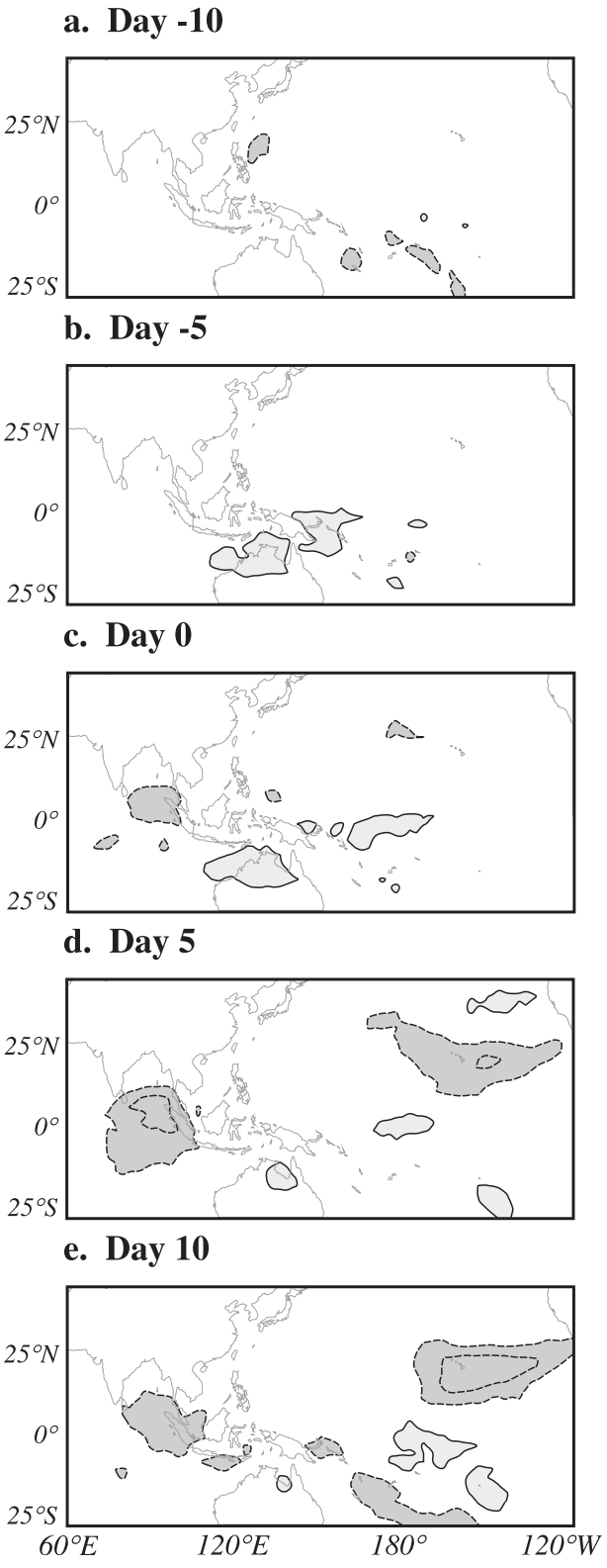

FIG. 12. Composite structure of OLR anomalies (W m^{-2}) associated with a jet retraction event at days (a) −10, (b) −5, (c) 0, (d) +5, and (e) +10. Solid (dashed) lines indicate positive (negative) OLR anomalies contoured and shaded every 10 W m^{-2} with the 0 line removed.

g. OLR

Figure 12 shows the composite OLR anomalies associated with jet retraction events. Negative (positive) OLR anomalies are associated with cold (warm) cloud-top temperatures and deep convection (the absence of deep convection). There are three features to note in this composite: a quasi-stationary negative OLR anomaly over Indonesia, a positive OLR anomaly that is first observed over Australia at day −5, and a large negative anomaly located in the central–eastern Pacific after the jet retracts. The negative OLR anomaly over Indonesia is first observed at day 0 (Fig. 12c) and indicates anomalous convection in that region. This anomaly intensifies and grows more expansive by day +10 (Figs. 12d,e), but it does not move. Since it is relatively stationary, it is most likely not related to the MJO, which has a characteristic wave speed of 5 m s^{-1}(Zhang 2005).

The large negative OLR anomaly located over the central/eastern Pacific after the jet retraction, strongly visible at day +5 and day +10 (Figs. 12d,e), is most likely an effect of altered storm-track activity related to the retraction of the jet. As shown in Fig. 10, and consistent with Otkin and Martin's (2004b) research on kona storm activity in the Pacific basin, storm-track activity in the central subtropical Pacific increases upon retraction of the jet. An increase in storm-track activity over the central Pacific would tend to increase convection and cloudiness in the region, as indicated by a negative anomaly in the OLR composite field. Also, there is a smaller positive anomaly located immediately to the northeast of the negative OLR anomaly at day +5 (Fig. 12c), which corresponds to a companion decrease in convective activity where the storm track was shown to have reduced activity (Fig. 10).

A large positive OLR anomaly, which is first apparent over northern Australia at day −5 (Fig. 12b), is the third feature in the OLR composite and is not easily explained. The positive anomaly moves gradually eastward through the jet retraction period (Figs. 12b–e) and is located in the tropical central Pacific at day +10 (Fig. 12e). A positive OLR anomaly in that location is consistent with a localized decrease in the strength of the Hadley cell compared to climatology that could contribute to a decrease in the intensity of the Pacific jet.

4. Summary and conclusions

a. Summary

The physical interactions between transient disturbances and the jet lie at the heart of the large-scale, midlatitude circulation. The low-frequency circulation (jet stream) is responsible for steering the transient synoptic

disturbances, whose individual paths compose the storm track. However, variations in the zonal extent of the jet are internally forced by the eddy heat and momentum fluxes of the very synoptic disturbances, whose trajectories comprise the storm track (Orlanski 1998; Lau 1988). Aside from such large-scale dynamical considerations, rapid, subseasonal, westward retractions of the Pacific jet are associated with increased cold-season subtropical cyclone activity in the central and eastern Pacific (Otkin and Martin 2004b). In addition, Higgins et al. (2000) have shown that the Pacific jet is zonally extended prior to extreme precipitation events along the West Coast of the United States.

Motivated by these connections, 28 yr of NCEP–NCAR reanalysis data have been employed in composite analysis of the evolution of the large-scale circulation associated with rapid retractions of the Pacific jet, a phenomenon that represents the dominant mode of variability of the 300-hPa zonal flow at midlatitudes. The analysis presented here has focused on 19 Pacific jet retraction events. The composite analysis perspective shows that the centers of extratropical circulation in the North Pacific basin undergo a complete reversal within a 2-week period in association with jet retractions as a dominant negative anomaly becomes a dominant positive anomaly across the North Pacific in both the 500-hPa geopotential height and SLP fields. The vertical superposition of these upper- and lower-level anomalies indicates that the circulation structures associated with a jet retraction are equivalent barotropic. The resulting anticyclonic anomalies are sprawling and intense with SLP anomalies of nearly 20 hPa and 500-hPa geopotential height anomalies of more than 200 m. The strong similarity between the upper-level geopotential height anomalies and a characteristic PNA pattern indicate that rapid retractions of the jet are associated with the rapid onset of a negative PNA pattern. The results are consistent with the composite 200–250-hPa Ertel PV anomaly field, in which a jet retraction event is characterized by the formation of a zonally elongated, meridionally oriented PV anomaly couplet in the central North Pacific that becomes increasingly isotropic in the jet exit region as the jet retracts.

Because of the large spatial scale over which jet retraction events occur, they also have been discussed in the context of the Pacific storm track, the East Asian winter monsoon (EAWM), and tropical diabatic heating. Variability in the Pacific storm track is found to accompany jet retraction events. When the jet is retracted, a substantial reduction in storm-track density occurs poleward and downstream of the climatological jet exit region, consistent with prior studies (e.g., Matthews and Kiladis 1999; Otkin and Martin 2004b) that have suggested that a retracted jet provides a weaker waveguide that allows the equatorward propagation of midlatitude disturbances into the subtropics of the central and eastern Pacific basin. Conversely, a zonally extended jet, which provides a strong waveguide, relegates synoptic-scale eddies to latitudes north of the jet axis (Matthews and Kiladis 1999).

The link between jet retraction events and break periods of the EAWM is less straightforward but nonetheless compelling. Based upon a composite study of eight surge and five break periods, Chang and Lau (1982) found that during cold surge (break) periods, the Pacific jet is accelerated (decelerated) and extended (retracted) while the Hadley circulation near Indonesia is strengthened (weakened). In the present study, two indices of the EAWM were examined in relation to the composite jet retraction event. Both monsoon indices show that jet retraction events tend to be preceded by EAWM break periods, with a reduction in zonal wind propagating downstream from the EAWM region into the central Pacific.

Finally, upon examination of composite OLR anomalies during jet retraction events, the link between jet retractions and anomalous tropical convection can been seen through the development of a large negative OLR anomaly over the central–eastern Pacific after the jet retracts, reflecting the increase in storm-track activity observed in that region. A positive OLR anomaly located immediately to its northeast is consistent with storm-track suppression poleward and downstream of the climatological jet in association with jet retractions. Two other features seen on the OLR composite are a quasi-stationary negative OLR anomaly located over the Indian Ocean, with a maximum amplitude at day +5, and a positive OLR anomaly over Australia, maximized at day 0. Only the positive OLR anomaly over Australia significantly precedes the jet retraction events. The physical connection between the Indonesian and Australian OLR anomalies and jet retraction events is not yet clear.

b. Possible mechanisms

Though characterizing the structure and evolution of jet retraction events has been the focus of the present study, there are connections to elements of the large-scale circulation that suggest physical mechanisms, operating in the jet exit region, that may underlie these rapid retractions.

Otkin and Martin (2004b) showed that active periods of subtropical cyclone activity associated with increased tropical convection over the Maritime Continent were accompanied by a significant westward retraction of the Pacific jet. Upon examination of the composite difference

zonal wind fields at 300 hPa between such active and inactive kona storm periods, they noted that periods in which the Pacific jet was retracted (i.e., substantially weaker westerlies were found in the jet exit region) were accompanied by stronger westerlies to the north and south of the jet axis [the spatial structure of their zonal wind anomalies (see their Fig. 14a) resembles Fig. 4 herein]. Hoskins et al. (1983) demonstrated that barotropic energy exchanges involving low-frequency eddies (of characteristic period greater than 10 days) located in the jet exit region act to weaken the zonal wind where it is strong and strengthen it where it is weak, increasing eddy kinetic energy at the expense of jet intensity. The response is a shorter, broader jet manifested as an easterly zonal wind anomaly at the axis of the jet exit region, flanked by westerly wind anomalies to the north and south. Interestingly, the EOF/PC analysis in Fig. 4 shows a strong anomaly of the zonal wind located at the jet exit region accompanied by oppositely signed anomalies to the north and the south. Taken together, the EOF analysis shown in Fig. 4, the corresponding wind pattern in Otkin and Martin (2004b), and the results of Hoskins et al. (1983) make a compelling case that barotropic instability is linked to jet retraction events.

Also, the role of deformation of the mean PV gradient likely plays an important role in the evolution of jet retraction events. As seen in the composite analysis of Ertel PV (Figs. 9c,d), a meridionally oriented PV anomaly couplet is located in the jet exit region as the jet retracts. Although initially zonally elongated, this couplet becomes more isotropic with time, likely as a result of deformation in the diffluent jet exit region. In addition to the deformation associated with the jet exit region mean circulation, the PV anomaly couplet has its own characteristic anomalous circulation: anticyclonic around the negative PV anomaly and cyclonic around the positive PV anomaly. The combination of these anomalous circulations acts to weaken the mean PV gradient to the west of the anomalies, as shown conceptually in Fig. 13.

The weakening of this upper-level PV gradient is closely related to the strength of the local vertical shear, as suggested by Davis and Bosart (2003) and Hulme and Martin (2009), who demonstrate, via the quasi-geostrophic (QG) potential vorticity, that the largest values of vertical shear will be collocated with the largest magnitudes of upper-level PV gradients. A local weakening of the PV gradient is therefore associated with a reduction of the vertical shear in the same region. In addition to this weakening of the upper-tropospheric PV gradient, the anomalous circulation would also impose anomalous easterly flow at the jet axis, which is consistent with jet retraction events.

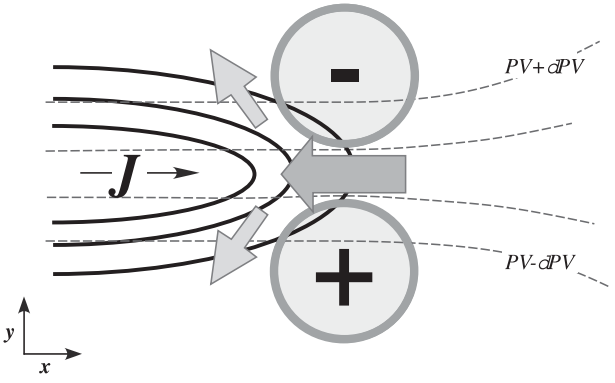

FIG. 13. Conceptual model of the effect of a meridional dipole of perturbation PV on the structure and circulation of the jet exit region during jet retraction events. Dashed lines are isertels of tropopause-level PV. Thick black lines represent schematic isotachs of the jet. Circular regions labeled "+" and "-" are perturbation PV features associated with jet retraction events (i.e. the PV dipole). Dark gray arrow is the perturbation easterly flow at the jet exit region arising from the meridional juxtaposition of the perturbation PV anomalies. Light gray arrows show the perturbation deformation associated with the PV dipole that weakens the PV gradient at and west of the jet exit region.

The analyses presented in this paper are mainly statistical in nature: composite analyses and linear regression analyses have been used to determine the large-scale structure and evolution of jet retractions. To systematically and quantitatively implicate specific mechanisms in forcing jet retraction events, a number of additional steps must be undertaken in future work. Employment of a case-study approach to several of the individual jet retractions would likely lead to greater insight into the nature of the underlying physical processes that govern these events. To better diagnose and examine the interactions between the high- and low-frequency components of the circulation during jet retraction events, piecewise tendency diagnosis, a diagnostic extension of quasi-geostrophic potential vorticity (QGPV) inversion (Lefevre 1995; Nielsen-Gammon and Lefevre 1996; Evans and Black 2003), will be employed in future work.

Acknowledgments. This work was supported by the National Science Foundation (Grants NSF-0806340 and NSF-0653795) and by the Graduate School at the University of Wisconsin—Madison. The careful reviews of two anonymous referees are greatly appreciated.

REFERENCES

Armstrong, R. L., and M. J. Brodzik, 1995: An earth-gridded SSM/I data set for cryospheric studies and global change monitoring. *Adv. Space Res.,* **16,** 155–163.

Bryson, R. A., 1994: The discovery of the jet stream. *Wis. Acad. Rev.,* (Summer), 15–17.

Caruso, S. J., and S. Businger, 2006: Subtropical cyclogenesis over the central North Pacific. *Wea. Forecasting,* **21,** 193–205.

Chang, C.-P., and K. M. W. Lau, 1980: Northeasterly cold surges and near-equatorial disturbances over the winter MONEX area during December 1974. Part II: Planetary-scale aspects. *Mon. Wea. Rev.,* **108,** 298–312.

——, and ——, 1982: Short-term planetary-scale interactions over the tropics and midlatitudes during northern winter. Part I: Contrasts between active and inactive periods. *Mon. Wea. Rev.,* **110,** 933–946.

Chang, E. K. M., S. Lee, and K. L. Swanson, 2002: Storm track dynamics. *J. Climate,* **15,** 2163–2183.

Chu, P. S., A. J. Nash, and F. Y. Porter, 1993: Diagnostic studies of two contrasting rainfall episodes in Hawaii: Dry 1981 and wet 1982. *J. Climate,* **6,** 1457–1462.

Davis, C. A., and L. F. Bosart, 2003: Baroclinically induced tropical cyclogegnesis. *Mon. Wea. Rev.,* **131,** 2730–2747.

Evans, K. J., and R. X. Black, 2003: Piecewise tendency diagnosis of weather regime transitions. *J. Atmos. Sci.,* **60,** 1941–1959.

Glickman, T. Ed., 2000: *Glossary of Meteorology*. 2nd ed. Amer. Meteor. Soc., 855 pp.

Higgins, R. W., and K. C. Mo, 1997: Persistent North Pacific circulation anomalies and the tropical intraseasonal oscillation. *J. Climate,* **10,** 223–244.

——, J. K. E. Schemm, W. Shi, and A. Leetmaa, 2000: Extreme precipitation events in the western United States related to tropical forcing. *J. Climate,* **13,** 793–820.

Hoskins, B. J., and D. J. Karoly, 1981: The steady linear response of a spherical atmosphere to thermal and orographic forcing. *J. Atmos. Sci.,* **38,** 1179–1196.

——, and P. J. Valdes, 1990: On the existence of storm tracks. *J. Atmos. Sci.,* **47,** 1854–1864.

——, I. N. James, and G. H. White, 1983: The shape, propagation and mean-flow interaction of large-scale weather systems. *J. Atmos. Sci.,* **40,** 1595–1612.

——, M. E. McIntyre, and A. W. Robertson, 1985: On the use and significance of isentropic potential vorticity maps. *Quart. J. Roy. Meteor. Soc.,* **111,** 877–946.

Hsu, H.-H., and J. M. Wallace, 1985: Vertical structure of wintertime teleconnection patterns. *J. Atmos. Sci.,* **42,** 1693–1710.

Hulme, A. L., and J. E. Martin, 2009: Synoptic- and frontal-scale influences on tropical transition events in the Atlantic basin. Part I: A six-case survey. *Mon. Wea. Rev.,* **137,** 3605–3625.

Jhun, J.-G., and E.-J. Lee, 2004: A new East Asian winter monsoon index and associated characteristics of the winter monsoon. *J. Climate,* **17,** 711–726.

Johnson, N. C., and S. B. Feldstein, 2010: The continuum of North Pacific sea level pressure patterns: Intraseasonal, interannual, and interdecadal variability. *J. Climate,* **23,** 851–867.

Kalnay, E., and Coauthors, 1996: The NCEP/NCAR 40-Year Reanalysis Project. *Bull. Amer. Meteor. Soc.,* **77,** 437–471.

Knutson, T. R., and K. M. Weickmann, 1987: 30–60 day atmospheric oscillations: Composite life cycles of convection and circulation anomalies. *Mon. Wea. Rev.,* **115,** 1407–1436.

Kodama, K., and G. M. Barnes, 1997: Heavy rain events over the south-facing slopes of Hawaii: Attendant conditions. *Wea. Forecasting,* **12,** 347–367.

Lau, K.-M., and M.-T. Li, 1984: The monsoon of East Asia and its global associations—A survey. *Bull. Amer. Meteor. Soc.,* **65,** 114–125.

Lau, N.-C., 1988: Variability of the observed midlatitude storm tracks in relation to low-frequency changes in the circulation pattern. *J. Atmos. Sci.,* **45,** 2718–2743.

Lefevre, R. J., 1995: Using the quasigeostrophic potential vorticity height tendency equation to diagnose the development of midtropospheric mobile troughs. Ph.D. thesis, Texas A&M University, 233 pp.

Liebmann, B., and C. A. Smith, 1996: Description of a complete (interpolated) outgoing longwave radiation dataset. *Bull. Amer. Meteor. Soc.,* **77,** 1275–1277.

Lyons, S. W., 1982: Empirical orthogonal function analysis of Hawaiian rainfall. *J. Appl. Meteor.,* **21,** 1713–1729.

Madden, R. A., and P. R. Julian, 1971: Detection of a 40–50 day oscillation in zonal wind in the tropical Pacific. *J. Atmos. Sci.,* **28,** 702–708.

——, and ——, 1994: Observations of the 40–50-day tropical oscillation—A review. *Mon. Wea. Rev.,* **122,** 814–837.

Matthews, A. J., and G. N. Kiladis, 1999: The tropical–extratropical interaction between high-frequency transients and the Madden–Julian oscillation. *Mon. Wea. Rev.,* **127,** 661–677.

——, B. J. Hoskins, and M. Masutani, 2004: The global response to tropical heating in the Madden-Julian oscillation during the northern winter. *Quart. J. Roy. Meteor. Soc.,* **130,** 1991–2011.

Moore, R. W., O. Martius, and T. Spengler, 2010: The modulation of the subtropical and extratropical atmosphere in the Pacific basin in response to the Madden–Julian oscillation. *Mon. Wea. Rev.,* **138,** 2761–2779.

Mori, M., and M. Watanabe, 2008: The growth and triggering mechanisms of the PNA: A MJO-PNA coherence. *J. Meteor. Soc. Japan,* **86,** 213–236.

Newman, M., and P. D. Sardeshmukh, 1998: The impact of the annual cycle on the North Pacific/North American response to remote low-frequency forcing. *J. Atmos. Sci.,* **55,** 1336–1353.

Nielsen-Gammon, J. W., and R. J. Lefevre, 1996: Piecewise tendency diagnosis of dynamical processes governing the development of an upper-tropospheric mobile trough. *J. Atmos. Sci.,* **53,** 3120–3142.

North, G. R., T. L. Bell, R. F. Cahalan, and F. J. Moeng, 1982: Sampling errors in the estimation of empirical orthogonal functions. *Mon. Wea. Rev.,* **110,** 699–706.

Orlanski, I., 1998: Poleward deflection of storm tracks. *J. Atmos. Sci.,* **55,** 2577–2602.

Otkin, J. A., and J. E. Martin, 2004a: A synoptic climatology of the subtropical kona storm. *Mon. Wea. Rev.,* **132,** 1502–1517.

——, and ——, 2004b: The large-scale modulation of subtropical cyclogenesis in the central and eastern Pacific Ocean. *Mon. Wea. Rev.,* **132,** 1813–1828.

Reiter, E. R., 1963: *Jet-Stream Meteorology*. University of Chicago Press, 515 pp.

——, 1967: *Jet Streams; How Do They Affect Our Weather?* Doubleday, 189 pp.

Schubert, S. D., and C.-K. Park, 1991: Low-frequency intraseasonal tropical–extratropical interactions. *J. Atmos. Sci.,* **48,** 629–650.

Serreze, M. C., 1995: Climatological aspects of cyclone development and decay in the Arctic. *Atmos.–Ocean,* **33,** 1–23.

——, F. Carse, R. G. Barry, and J. C. Rogers, 1997: Icelandic low cyclone activity: Climatological features, linkages with the NAO, and relationships with recent changes in the Northern Hemisphere circulation. *J. Climate,* **10,** 453–464.

Simpson, R. H., 1952: Evolution of the kona storm, a subtropical cyclone. *J. Meteor.,* **9,** 24–35.

Valdes, P. J., and B. J. Hoskins, 1989: Linear stationary wave simulations of the time-mean climatological flow. *J. Atmos. Sci.,* **46,** 2509–2527.

Wallace, J. M., and D. S. Gutzler, 1981: Teleconnections in the geopotential height field during the Northern Hemisphere winter. *Mon. Wea. Rev.,* **109,** 784–812.

Weickmann, K. M., G. R. Lussky, and J. E. Kutzbach, 1985: Intraseasonal (30–60 day) fluctuations of outgoing longwave radiation and 250 mb streamfunction during northern winter. *Mon. Wea. Rev.,* **113,** 941–961.

Wu, B. W., R. Zhang, and R. D'Arrigo, 2006: Distinct modes of the East Asian winter monsoon. *Mon. Wea. Rev.,* **134,** 2165–2179.

Wu, M. C., and J. C. L. Chan, 1997: Upper-level features associated with winter monsoon surges over south China. *Mon. Wea. Rev.,* **125,** 317–340.

Zhang, C., 2005: Madden-Julian oscillation. *Rev. Geophys.,* **43,** RG2003, doi:10.1029/2004RG000158.

Zhang, Y., K. R. Sperer, and J. S. Boyle, 1997: Climatology and interannual variation of the East Asian winter monsoon: Results from the 1979–95 NCEP/NCAR reanalysis. *Mon. Wea. Rev.,* **125,** 2605–2619.

Zhu, Y., 2008: An index of East Asian winter monsoon applied to the description of China's mainland winter temperature changes. *Acta Meteor. Sin.,* **22,** 522–529.